XL CILAMCE
IBERO-LATIN AMERICAN CONGRESS ON COMPUTATIONAL METHODS IN ENGINEERING
NOVEMBER 11-14, 2019
Praiamar Natal Hotel & Convention
Natal, RN-BRAZIL

A FINITE ELEMENT APPROACH TO UPPER BOUND SOLUTIONS FOR ULTIMATE LOADS OF PLATES AND SLABS

Michael Parisotto
mica.parisotto@gmail.com
Federal University of Rio Grande do Sul
Vanessa F. Pasa Dutra
Samir Maghous
pasa.dutra@ufrgs.br
samir.maghous@ufrgs.br
Department of Civil Engineering, Federal University of Rio Grande do Sul
Av. Osvaldo Aranha, 99, Centro, Porto Alegre, 90035-190, Rio Grande do Sul, Brazil

Abstract. Structural engineering projects involves the elements design considering the ultimate limit state (ULS) conditions and the service limit state (SLS) check. The ULS is characterized by the exhaustion of the strength capacity of the entire structure or some specific regions. SLS conditions should be checked to ensure durability of the structure, maintenance of non-structural elements appearance and integrity, which influence users comfort as well as the buildings functionality. No additional loading can be sustained by the structure beyond the ultimate state conditions. The present work aims at analyzing the ULS of plates and slabs under predominating flexion through numerical evaluation of their load capacities. The combination of the kinematic approach of limit analysis theory (LAT) with the finite element method (FEM) enabled the development of a computational tool that allows for assessing the failure load of plates and slabs with arbitrarily geometry and associated support conditions when subjected to different loading modes (surface, linear and concentrated). Adopting the normal deflection rate as main variable that controls the failure mechanism, six-node triangular finite elements were used for geometry and kinematics discretization. The numerical determination of ultimate load of the structure relies upon a minimization procedure. The latter is achieved by Sequential Quadratic Programming (SQP) method, which is an iterative method for constrained nonlinear optimization. The developed finite element tool also allows the analysis of the failure mechanism of plates and slabs and visualization through the software of pre-and post-processing GiD®. For the validation of the proposed analysis methodology (LAT + FEM) and associated computational implementation, analytical results of various slab and plate configurations and their respective rupture mechanisms were favorably compared with the numerical predictions. Comparison with available approaches are also presented, thus indicating the ability of the developed numerical tool to accurately assess the ultimate loads and failure mechanisms of bending plates or slabs.

Keywords: Plates and Slabs; Failure; Ultimate Limit State, Limit Analysis Theory, Finite Element Method

1 Introduction

Structural engineering projects involves the elements design considering the ultimate limit state (ULS) conditions and the service limit state (SLS) check. Such procedures are widely executed with the support of commercial software programs, which are used to assist engineers in the decision-making process. The ULS is characterized by the exhaustion of the strength capacity of the entire structure or some specific regions, its occurrence determines the structure use stoppage. It is a not expected condition to reach, so the strength capacities of materials are lessened while the loads are increased. The SLS conditions are verified so that the structural durability, non-occurrence of damage to non-structural elements, the maintenance of the aesthetics, that influence the user well-being and building functionalities are guaranteed. Many software tools use numerical methods that analyze the structural model with the basic assumption that the structure materials have an elastoplastic behavior and that the deformations are within the elastic regime.

Plates and slabs are elements with a plane surface, in which one of the dimensions (the thickness) is significantly smaller than the other two dimensions (length and width) and are mostly subjected to loads that are perpendicular to its reference medium plane. The term "slab" is generally used to define plates made of reinforced concrete. Between the existent methods to calculate ultimate loads in Slabs, the Yield-Line Theory (Johansen [1], Jones and Wood [2], Langendock [3]), predicts that in the imminence of collapsing, yield lines are formed at the regions of maximum bending moment on the slab, which is constant along these lines, with the assumptions of deformations disregarding throughout the slab and the separation of the slab in plane regions that can only experiment pure rotation movements. Such yield lines, that can be referenced here as plastic hinges, indicate the path that cracks will appear in reinforced concrete elements, where the reinforcement bars will be at a yielding limit state. Generally, a simplified collapse configuration is presumed, therefore, easing the determination of collapsing bending moments and ultimate load values.

This project was generated in the context of the ULS of structures, specifically of plates and slabs, using the Limit Analysis Theory (LAT) and the Finite Element Method (FEM). Limit Analysis is concerned with the ultimate loads determination, it does not evaluate the behavior of structures in service or throughout their loading path, but only just before collapse, or failure. It is based on the lower limit (static) and upper limit (kinematic) theorems, which provide lower and upper limits of the ultimate loads of structures (Chen and Han [4], Salençon [5], Salençon [6]). It is noteworthy that the conventional design of structures, i.e. consideration of elastic behavior, is more conservative and less economical when compared to designing in the ULS. The FEM is a widely known method used to solve the most diverse problems of different areas of knowledge (Zienkiewicz et al. [7], Rao [8], Reddy and Gartling [9]). The combination of FEM and LAT allows to numerically determine the occurrence of collapse configurations in plates and slabs of any shape and support conditions, subjected to several types of loading, considering deformations and their discontinuities.

The purpose of this study was to develop a computational tool based on the FEM and the LAT, which helps to design, verify, understand the collapse configurations of plane structural elements, such as solid reinforced concrete slabs, with several geometries, and especially in obtaining the load capacity of this type of structure. Thus, an algorithm for the determination of ultimate load was developed and implemented. Its validation was possible by the comparison with results obtained from models available in the literature.

Notations: throughout the paper, the following notations are adopted: a scalar, $\vec{a}$ vector, $\underline{\underline{a}}$ second-order tensor.

2 Plates and Slabs under Bending

2.1 Plate model

A plate is a three-dimensional solid that has a characteristic dimension (thickness e) smaller than the others (contained in the longitudinal plane l_x and l_y) (Fig. 1(a)). Thus, it can be analyzed with a two-dimensional model (Fig. 1(b)). Its geometric description is made by its medium plane definition, which is perpendicular (or normal) to its transverse fibers (Fig. 1(b)).

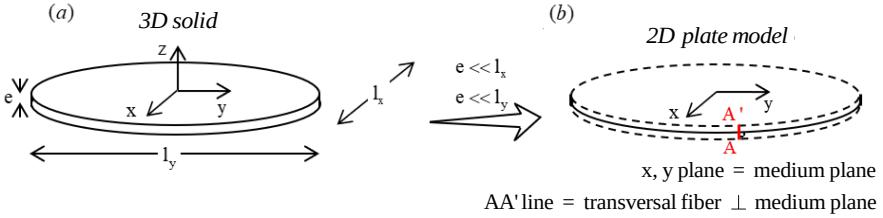

Figure 1. Plate geometric description.

In three-dimensional solids, the description of internal solicitations is given by the stress state at any point of the element, i.e. by the stress tensor $\underline{\underline{\sigma}}$. For plate elements without torsion, the internal stresses are of three types: normal $\underline{\underline{N}}$ (or membrane) and shear $\vec{V}$ forces, and bending moment $\underline{\underline{M}}$. The following equations

$$div\underline{\underline{N}} + \vec{f} = 0, \quad \underbrace{div\vec{V} - p = 0 \quad e \quad div\underline{\underline{M}} + \vec{V} = 0}_{\frac{\partial^2 M_{xx}}{\partial x^2} + \frac{\partial^2 M_{yy}}{\partial y^2} + 2\frac{\partial^2 M_{xy}}{\partial x \partial y} + p = 0 \ \ (Equação \ \ da \ \ Placa)}, \tag{1}$$

translate the plate equilibrium. $\vec{f}$ and $\vec{p}$ are force densities, parallel and perpendicular to the plate medium plane, respectively, defined by surface [N/m²] or length [N/m] units. Eq. (1) indicate that the membrane stresses are uncoupled from bending and shear stresses, the latter being coupled.

2.2 Kinematics of Plates and Slabs

In this work, there will be considered only the bending movements of the plates, i.e. for which the axial strain rate is null. Plate bending kinematics are defined by the displacement rate $\dot{v}\vec{e}_z$, the rate of rotation of the fiber normal to the medium plane $\vec{\dot{\theta}} = \dot{\theta}_x\vec{e}_x + \dot{\theta}_y\vec{e}_y$ and the rate of rotation of the medium plane $\vec{w} = grad\dot{v} \wedge \vec{e}_z$ (Fig. 2).

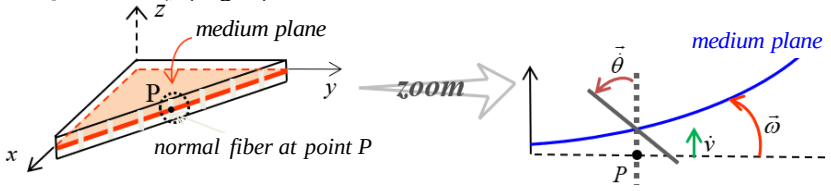

Figure 2. Plate kinematic description.

In plates or slabs subjected to bending, fractures are observed along lines (or hinges) separating stiff blocks, making it possible to identify concentrated rotations (i.e., discontinuity of rotation) along these hinges. To model this type of local rupture it is necessary to introduce the notion of rotational rate discontinuity (or concentrated rotation). $\dot{v}$ must remain continuous along the plate (condition required for the displacement rate), but its gradient may be discontinuous along a line $\mathcal{L}$ (Fig. 3). The plate rotation rate discontinuity (medium plane) $[\vec{\omega}]$ is calculated by choosing the vector $\vec{n}$ perpendicular to the rotation rate discontinuity line $\mathcal{L}$ at point P (Fig. 3) of (1) $\rightarrow$ (2) through the following expression:

$$\vec{\omega} = \text{grad}\,\dot{v} \wedge \vec{e}_z \quad \Rightarrow \quad [\vec{\omega}] = \vec{\omega}_2 - \vec{\omega}_1 = [\text{grad}\,\dot{v}] \wedge \vec{e}_z\,, \quad \text{with} \tag{2}$$

$$\forall\ \text{P} \in \mathcal{L} \qquad [\ \text{grad}\ \dot{v}\ ] = \text{grad}\ \dot{v}\ |_{(2)} - \text{grad}\ \dot{v}\ |_{(1)}\,. \tag{3}$$

According to Hadamard's Lemma $[\vec{\omega}] = [\omega]\,\vec{t}$, the vector $\vec{t}$ being tangential to the line of rotation rate discontinuity at point P.

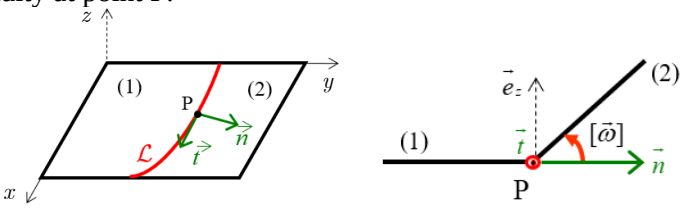

Figure 3. Line of discontinuity of the rotation rate in a plate (a) and rotation rate discontinuity of the plate medium plane (b).

2.3 External Action and Deformation Powers and Virtual Power Theorem

A plate structure is considered, subjected to punctual or linear surface forces. The vector $\vec{Q} = \ Q_1, Q_2, \ldots, Q_n\ $ is formed by the structure load parameters set, which includes every type of load that the structure may undergo (permanent, accidental loads). It is also considered a virtual movement ($m.v.$) compatible with the boundary conditions of the plate and defined by the displacement $\dot{v}\vec{e}_z$ and rotation rates $\dot{\vec{\theta}}$. The work rate or virtual power of external actions P_{ext} is:

$$P_{ext} = \vec{Q} \cdot \dot{\vec{q}} \tag{4}$$

where $\dot{\vec{q}}$ is the generalized virtual displacement rate vector of the structure.

The deformation power P_{def}, in turn, is the sum of the portions referring to the shear stresses $\vec{V}$ and bending moment $\underline{\underline{M}}$, as well as the contribution of the rotation rate discontinuity $[\vec{\omega}]$:

$$\forall\ \dot{v}, \dot{\vec{\theta}} \quad m.v.,\ P_{def} = \int_{placa} \vec{V} \cdot \underbrace{\vec{e}_z \wedge \left(\vec{\omega} - \dot{\vec{\theta}}\right)}_{\dot{\vec{\varepsilon}}_V} + \underline{\underline{M}} : \underbrace{\text{grad}\left(\vec{e}_z \wedge \dot{\vec{\theta}}\right)}_{\dot{\underline{\underline{\varepsilon}}}_M}\ dS + \underbrace{\int_{\mathcal{L}} M_{nn}[\vec{\omega}]\,ds}_{\substack{\text{rotation rate} \\ \text{discontinuity contribution}}} \tag{5}$$

where $\dot{\vec{\varepsilon}}_V$ refers to the shear deformation rate of the plate. $\dot{\underline{\underline{\varepsilon}}}_M$ is the plate bending strain rate. $M_{nn} = \vec{n} \cdot \underline{\underline{M}} \cdot \vec{n}$ is the moment that causes the rotation of (2)/(1) around the line $\mathcal{L}$.

The Kirchhoff-Love condition for plates is analogous to the Navier-Bernoulli condition for beams. It postulates that the transverse fiber remains normal to the medium plane of the plate during its movement. Thus, the set of motions $\mathcal{F}$ that satisfy the Kirchhoff-Love condition are the bending motions for which the plate rotation (i.e., the average fiber) $\vec{\omega}$ is equal to the rotation of the transverse fiber (i.e., the perpendicular or normal fiber) $\dot{\vec{\theta}}$ and therefore the shear strain rate $\dot{\vec{\varepsilon}}_V$ is zero and the bending strain rate $\dot{\underline{\underline{\varepsilon}}}_M$ is equal to the plate curvature rate $\dot{\underline{\underline{\chi}}} = \ \text{grad}\ \ \text{grad}\,\dot{v}\ $. For such motions, the deformation power P_{def} is composed of the bending and the rotation rate gradient portion $\dot{\underline{\underline{\chi}}}$ and the bending and rotation rate discontinuities portion $[\dot{\theta}]$. There is no shear contribution:

$$\forall\ \ \dot{v}, \dot{\vec{\theta}}\ \ \in \mathcal{F}, \qquad P_{def} = \int_{placa} \underline{\underline{M}} : \dot{\underline{\underline{\chi}}}\ dS + \int_{\mathcal{L}} M_{nn}\ [\dot{\theta}]\ \ ds\ \ . \tag{6}$$

The virtual power theorem, as well as the virtual work theorem, expresses in a dual way the equations of equilibrium (Eq. (1)) and, therefore, it is similar to equilibrium. The VPT can be expressed as: “For any virtual motion, the power of external forces is equal to the power of deformation” or yet:

$$\forall\ \ \dot{v}, \dot{\vec{\theta}}\ \ \in \mathcal{F}, \qquad \vec{Q} \cdot \dot{\vec{q}}\ = \int_{placa} \underline{\underline{M}} : \dot{\underline{\underline{\chi}}}\ dS + \int_{\mathcal{L}} M_{nn}\ [\dot{\theta}]\ \ ds\,, \tag{7}$$

when bending motions that satisfy the Kirchhoff-Love condition are considered.

2.4 Plates Failure Domain

The strength criterion defines the strength capacity of the material. It constitutes a limitation on the allowable internal stresses of the material. Its general form for the case of slabs and plates without torsion is $f(\underline{\underline{N}},\vec{V},\underline{\underline{M}}) \leq 0$. In engineering practice, it is often and legitimate to disregard the influence of normal and shear stresses on the resistant capacity of plates/slabs. This consideration physically represents the fact that the bending strength is much lower than the normal stress strength and that the shear strength. This study is interested in plates and slabs under bending for which the strength to normal and shear forces is much higher than the bending strength and, therefore, it is the bending that dictates the design in the ULS (hypothesis confirmed by experimental observations of slabs and plates collapses under bending). Thus, in this case, it is considered only a limitation on bending $f(\underline{\underline{M}}) \leq 0$, i.e. $f(M_{xx}, M_{yy}, M_{xy}) \leq 0$, or even $f(M_1, M_2, \theta) \leq 0$, being M_1 and M_2 the principal bending moments and θ the principal direction. When it comes to isotropic material, there is no dominant direction and, therefore, the strength criterion depends only on the principal moments, i.e. $f(M_1, M_2) \leq 0$.

An alternative way to represent the strength domain is through its support functions. In the case of the bending strength criterion, its support functions $\Pi(\underline{\underline{\dot{\chi}}})$ and $\Pi([\dot{\theta}])$ are:

$$\Pi(\underline{\underline{\dot{\chi}}}) = \sup_{f(\underline{\underline{M}}) \leq 0} \underline{\underline{M}} : \underline{\underline{\dot{\chi}}} \quad e \quad \Pi([\dot{\theta}]) = \sup_{f(\underline{\underline{M}}) \leq 0} M_{nn}[\dot{\theta}] \qquad (both\ independent\ of\ \underline{\underline{M}}) . \tag{8}$$

Each failure criterion has expressions and support functions that characterize them. Criteria commonly employed for plates made of isotropic materials are, for example, the Tresca, von Mises, and Johansen criteria. The latter was the criterion applied in this study. It was conceived experimentally for reinforced concrete slabs built with reinforcement layers. The upper layer undergoes negative bending, while the lower layer undergoes positive bending. This criterion allows the consideration of different upper and lower layers and is represented by the following equation:

$$f(\underline{\underline{M}}) \leq 0 \quad \Leftrightarrow \quad -M_0^- \leq M_i \leq M_0^+ \qquad i = 1, 2 . \tag{9}$$

where, M_0^+ e M_0^- are the limit in positive and negative bending, respectively. M_1 and M_2 are the principal bending moments (eigenvalues of $\underline{\underline{M}}$), or even, by the support functions:

$$\begin{cases} \Pi(\underline{\underline{\dot{\chi}}}) = \max\ M_0^+\ \dot{\chi}_1\ ,\ -M_0^-\ \dot{\chi}_1\ + \max\ M_0^+\ \dot{\chi}_2\ ,\ -M_0^-\ \dot{\chi}_2 \\ \Pi([\dot{\theta}]) = \max\ M_0^+\ [\dot{\theta}]\ ,\ -M_0^-\ [\dot{\theta}] \end{cases} . \tag{10}$$

where, $\dot{\chi}_1$ and $\dot{\chi}_2$ are the principal curvature rates.

3 Limit Analysis of Plates and Slabs

Limit Analysis is concerned with ultimate loads determination. It considers compatibility between equilibrium and strength conditions of materials or structures. The solution of a Limit Analysis problem, i.e. the determination of the domain of potentially safe loads *K* of the structure, can be achieved by applying two distinct approaches: the Static Approach and the Kinematic Approach.

3.1 Static definition of *K*

A load set $\vec{Q}$ will be potentially safe if there is a distribution of internal stresses equilibrating it and satisfying the strength criterion at every point of the structure:

$$\vec{Q}\ \ potentially\,safe\ \ (\text{i.e. } \vec{Q} \in K) \ \Leftrightarrow\ \exists\ (\underline{\underline{M}})\ such\,that\ \begin{cases} (\underline{\underline{M}})\ \ equilibrate\ \ \vec{Q}\ \ (Equilibrium) \\ \forall\ (x,y)\ f\big(\underline{\underline{M}}(x,y)\big) \leq 0\ \ (Strength) \end{cases} . \tag{11}$$

The domain of potentially safe loads *K* for the structure is formed by the set of $\vec{Q}$ satisfying Eq.

(11). Also, $K \in \mathbb{R}^n$, where *n* is the number of load parameters. A direct application of the static definition of K leads to lower limits of ultimate loads.

3.2 Kinematic definition of *K*

A load set $\vec{Q}$ will be potentially safe if there is a distribution of internal stresses and, for any virtual motion, the power of external forces is equal to the deformation power, satisfying the strength criterion through every point of the structure:

$$\vec{Q} \quad potentially\,safe \;\; (\text{i.e. } \vec{Q} \in K) \Leftrightarrow \exists \; (\underline{\underline{M}}) \; such \; that \begin{cases} \forall \;\; \dot{v}, \vec{\dot{\theta}} \;\; \in \mathcal{F} \qquad P_{ext} = P_{def} \\ \forall \; (x,y) \qquad f\left(\underline{\underline{M}}(x,y)\right) \leq 0 \end{cases} . \quad (12)$$

The kinematic theorem states that:

$$\vec{Q} \;\; \text{suportável} \Rightarrow \forall \;\; \dot{v}, \vec{\dot{\theta}} \;\; \in \mathcal{F} \qquad P_{ext} \leq P_{rm} = \int_{placa} \Pi\left(\underline{\underline{\dot{\chi}}}\right) \; dS + \int_{\mathcal{L}} \Pi\left([\dot{\theta}]\right) ds \quad (13)$$

where P_{rm} is the maximum resistant power (or rate of work). The kinematic theorem provides a necessary condition for the structure stability. An application of the kinematic approach provides upper limits of the ultimate loads.

4 Numerical Approach via Finite Element Method

For plates analyzed through a two-dimensional model, the analysis parameter, in the problems proposed in this study, is the orthogonal displacement to the plate or the vertical or maximum displacement. The discretization considered for the Finite Element Method (FEM) solution was made with quadratic triangular elements (6 nodes), with one degree of freedom (DOF) per node, which represents the vertical nodal displacement. The problem is similar to a plate heat conduction problem, with only one DOF per node.

4.1 Displacement, Rotation and Curvature

In this section, the equation of vertical displacement for each element is presented, as a function of nodal displacements, and from this, the rotation and bending deformation, or curvature, for each element, which constitute the kinematic parameters necessary for the solution, of the applied method. The displacement, rotation and curvature at any point of a 6-node element is described by:

$$v = \sum_{i=1}^{6} L_i(x,y) \cdot v_i \; , \; \vec{\theta} = \overrightarrow{grad(v)} \times \vec{e_z} \;\; \text{e} \;\; \underline{\underline{\chi}} = grad(\overrightarrow{grad(v)}) \quad (14)$$

where L_i are the interpolation (or shape) functions of the quadratic triangular element. $\overrightarrow{grad(v)}$ is the gradient of v, which depends on the derivatives $\partial L_i / \partial x$ and $\partial L_i / \partial y$. $grad(grad(v))$ is the gradient of $grad(v)$, which depends on the derivatives, $\partial^2 L_i / \partial x^2$, $\partial^2 L_i / \partial y^2$ and $\partial^2 L_i / \partial xy$. The expressions of L_i and its derivatives, which are necessary for the calculation of v, $\vec{\theta}$ and $\underline{\underline{\chi}}$, applied in the present work, can be found in Parisotto [10].

4.2 Discretization with Finite Elements

Generally, according to the Kinematic Theorem, the problem to be solved for a generic plate subjected to a load $\vec{Q}$ is $P_{ext} \leq P_{rm}$, where P_{ext} and P_{rm} are defined in Eq. (4) and (13), respectively. For a finite element discretized plate, containing *n* elements, and *m* interfaces between elements or fixed edges, we rewrite:

$$P_{rm} = \sum_{i}^{n} \Pi_i (\dot{\underline{\underline{\chi}}}) \cdot S_i \; + \; \sum_{j}^{m} \Pi_j ([\dot{\theta}]) \cdot s_j \tag{15}$$

where S_i is the area of element *i* and s_j is the length of interface *j*. These parameters are calculated through their nodes coordinates. To find a load limit for the plate, we rewrite Eq. (13):

$$\vec{Q} \leq \frac{P_{rm}}{\vec{\dot{q}}} \tag{16}$$

To obtain an upper load limit Q^+, P_{rm} is minimized as a function of the plate nodal displacements n_i. Therefore, the minimization problem to be solved is

$$Q^+ = \min_{v_i} \; P_{rm} \quad , \tag{17}$$

subject to the restriction on nodal displacement rates $\vec{\dot{q}} = 1$.

4.3 Program Structure

The program structure can be seen in Fig. 4.

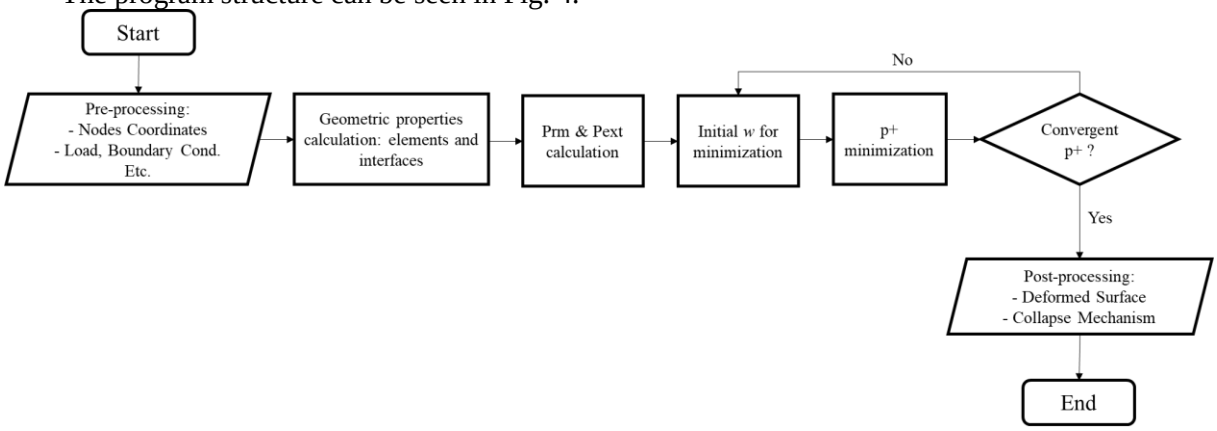

Figure 4. Software tool flowchart.

Pre and post processing were performed with help of *GiD*® software, in its free trial version, which allows to model meshes up to 10^3 nodes. The program initially executes the mesh file reading routines, which return the parameters of quantity, connectivity, area and interface between elements, quantity, and node coordinates. In sequence, it executes the routines to calculate the derivatives of shape functions of the elements, which are inherent to the mesh geometry, the routines for the calculation of P_{rm} and P_{ext}, and then, the function to be minimized and the constraints are defined to calculate the ultimate load. The minimization algorithm assigns values v_i to the nodal displacement vector, subjected to the restriction $\vec{\dot{q}} = 1$. With such values of v_i, the value of P_{rm}, is calculated according to Eq. (15) and the objective function P_{rm}/P_{ext} is minimized, which returns an upper limit value of Q^+, or p^+ in the case of distributed loads. Consequently, the values of v_i that minimize the problem represent the collapse configuration of the analyzed plate, or collapse mechanism. From these, we calculate the isovalues of $\Pi([\dot{\theta}])$ for each interface, and $\Pi(\dot{\underline{\underline{\chi}}})$ for each element, allocating these values for each node of the mesh, so that it is possible to visualize the determined collapse mechanism that can be viewed with *GiD*®.

The programming language used was Python, a high-level language developed to improve code reading and verification, thus enabling a more efficient interpretation for new users. Its libraries are open source, with a large and active community of users from around the world, who optimize and adapt the functions created to improve problem solving. For this work, one of the most important functions is the minimization of the multivariable function that is found, dependent on the

displacement of each node from the analyzed mesh. Therefore, a language with extensive (and easily accessible) optimization routines, such as Python, is required.

The minimization method used was an Sequential Quadratic Programming (SQP) method, which is defined as iterative for nonlinear constrained optimization. The SQP methods solve a sequence of optimization subproblems, referring to quadratic approximations of the original function, formulated through linear constraint conditions. If there are no constraints on the problem at hand, the SQP methods resemble Newton's method to find a point where the gradient of the function cancels out. Among Python libraries, the one that best meets the code needs is the SciPy library, specifically the scipy.optimize package, which contains several optimization methods. The constrained nonlinear optimization method for minimizing multivariable functions available in this library is the Sequential Least Squares Quadratic Programming (SLSQP) method, which applies the least squares method to solve quadratic subproblems that are iteratively generated.

5 Numerical Upper Bound Solutions for Ultimate Loads of Some Slabs

In this section, the slabs analyzed and their results are presented. Initially, simple geometric and loading configurations were tested, which the exact solutions or whose analytical solution of the kinematic approach from the LAT are known. Subsequently, problems without exact analytical solution were analyzed, such as L or T-shaped slabs. The validation of the proposed program was done by comparing the obtained numerical and the known analytical results. Although the developed tool allows the calculation of Von-Mises plates, the analyzes carried out consider slabs whose strength is characterized by the Johansen strength criterion. The values considered for the moment of rupture ($-M_0^-$ and M_0^+), were arbitrated according to the order of magnitude of M_0 for a von-Mises plate $M_0 = \sigma_o \ e^2/4$. Considering a plate of thickness $e = 10cm$ and uniaxial resistance $\sigma_o = 400MPa$, $-M_0^- = M_0^+ = M_0 = 1MNm / m$. This value was considered in all analyzed situations.

5.1 Modelagem de Lajes com Solução Exata

Square Slab subjected to distributed load simply supported on the boundary. This is a particular case of rectangular slabs. Their collapse mechanism and the exact solution are known, as both approaches of the limit analysis, static and kinematic, lead to the same solution, that in the case of a Johansen slab, is $p^+ = 6M_o/a^2$. The kinematic approach for this case characterizes the 4-rotation block collapse mechanism, as can be seen in Fig. 5.

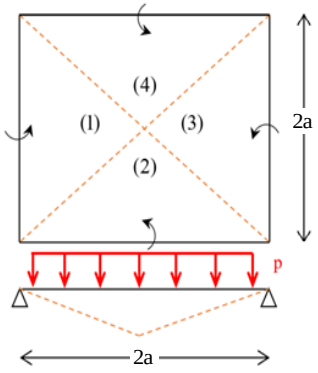

Figure 5. Square slab and the 4-rotation block collapse mechanism.

For the numerical solution (software tool), a square slab of 10m x 10m (i.e. $a = 5m$) was considered. The exact result in this case is $p^+ = 0,24MN / m^2$. Two finite element meshes (Fig. 6) were analyzed: 4 and 208 elements (free version of *GiD*® software imposed limitation).

The developed tool result for the 4 elements case was $p^+ = 0.240002899$ and for the 208 elements case was $p^+ = 0.262883411$. In addition, through the *GiD*® it was possible to visualize the deformed surface represented by the minimized nodal displacements, as shown in Fig. 7.

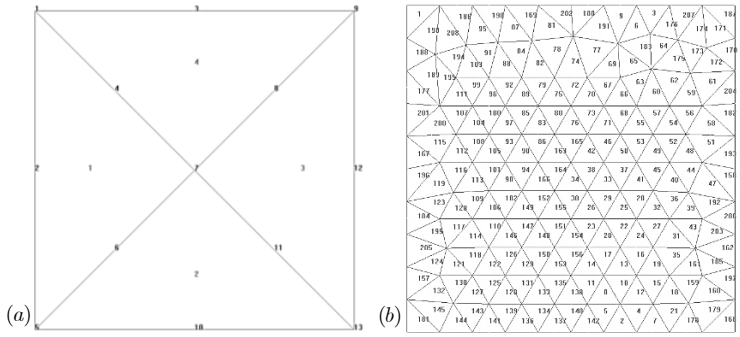

Figure 6. Square slab mesh (a) 4 and (b) 208 elements. Source: *GiD*®

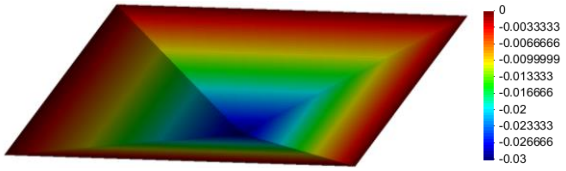

Figure 7. Deformed square slab, 4-element mesh. Source: *GiD*®

The program also allows the visualization of the isovalues of $\Pi([\dot{\theta}])$ for each interface, which represent the regions of the slab where rotation discontinuities occur, and the isovalores of $\Pi(\dot{\chi})$ for each element, which represent the occurrence or not of bending deformation, the latter case refers to the situations of stiff blocks in rotation in the collapse mechanism. Figures 8(a) and 8(b) respectively represent the isovalues of $\Pi([\dot{\theta}])$ and $\Pi(\dot{\chi})$ for the 4 elements case. Figures 9(a) and 9(b) respectively represent the isovalues of $\Pi([\dot{\theta}])$ and $\Pi(\dot{\chi})$ for the 208 elements case.

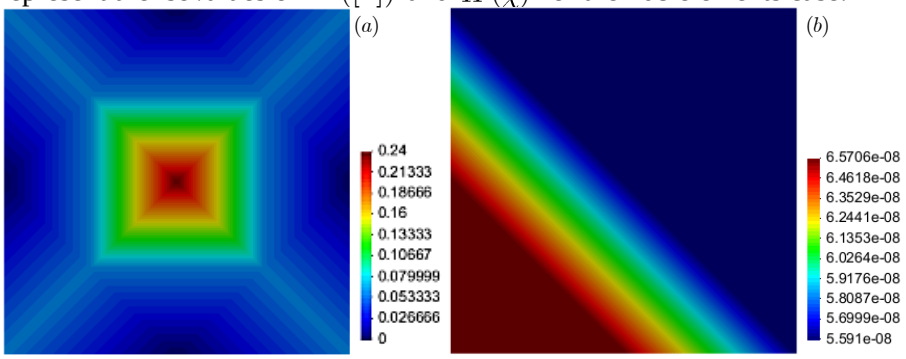

Figure 8. Isovalues of (a) $\Pi([\dot{\theta}])$ and (b) $\Pi(\dot{\underline{\underline{\chi}}})$ for a square slab (4 elements)

Figures 7, 8(a) and 8(b) show the expected collapse mechanism of 4 rotating rigid blocks. Such verification is possible by obtaining linear displacements (Fig. 7), rotational discontinuities at expected locations (Fig. 8(a)) and non-significant values (in the order of 10^{-8}) of bending deformation (Fig. 8(b)). Therefore, the mechanism for this geometric, load and boundary conditions configuration is characterized only by rotation discontinuities, or plastic hinges as expected.

Figure 9(a) shows the tendency of rotation discontinuities to characterize the exact collapse mechanism, however, due to the adopted distribution of triangular elements, some discontinuity lines adapt to the interfaces, following a different path from that previously observed when considering only 4 elements. It can be seen from Fig. 9(b) that near the most expressive lines of discontinuity, bending deformation occurs, somewhat compensating for the discontinuities in the numerically obtained collapse mechanism. In addition, the formation of rigid blocks in the dark blue areas is observed, which also characterizes the expected collapse mechanism. The 9.53% difference between numerical and exact solutions of p^+ is probably linked to the fact that the mesh used does not allow the formation of the exact collapse mechanism, as found previously, with the 4-element mesh.

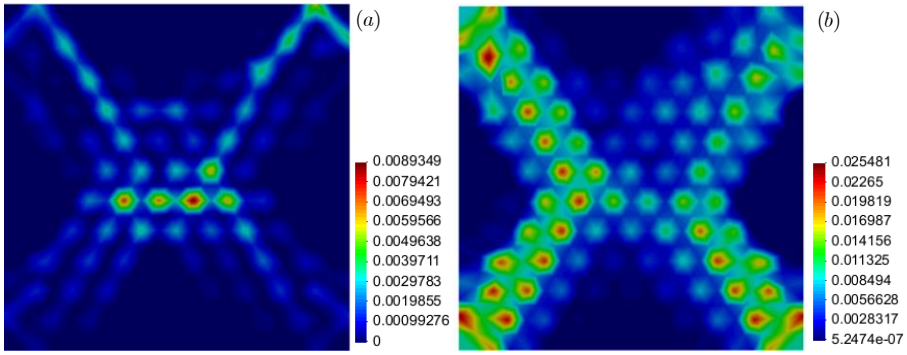

Figure 9. Isovalues of (a) $\Pi([\dot{\theta}])$ and (b) $\Pi(\underline{\underline{\dot{\chi}}})$ for a square slab (208 elements)

Square Slab subjected to distributed load fixed on the boundary. An upper loading limit for the slab with this type of geometry, load and boundary conditions, and strength characterized by the Johansen criterion, is $p^+ \leq 6\ M_0^- + M_0^+\ \big/ a^2$, obtained by considering hinges on the diagonals and along the fixed borders of the structure.

For the software tool numerical solution, a square slab of 10m x 10m (i.e. $a = 5m$) was considered. The result for these conditions is $p^+ = 0,48MN\ /\ m^2$. In this case, only one finite element mesh was considered: 208 elements, equal to that used for the simply supported square slab case (Fig. 6(b)). The result found by the software through minimization for the 208-element case was $p^+ = 0.475172371$. Figures 10(a) and 10(b) respectively represent the isovalues of $\Pi([\dot{\theta}])$ and $\Pi(\underline{\underline{\dot{\chi}}})$ for the 208 elements case.

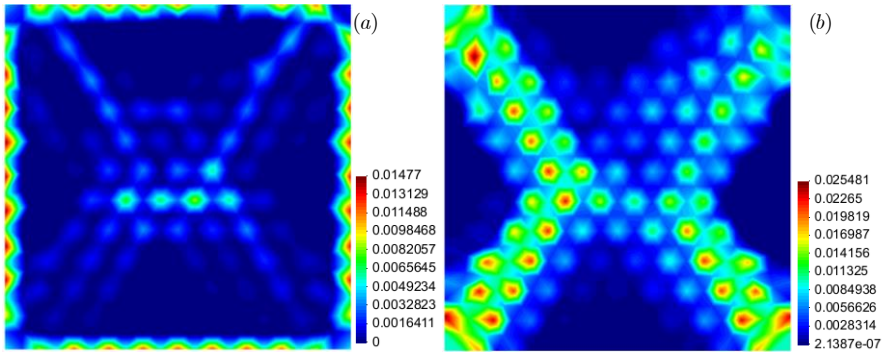

Figure 10. Isovalues of (a) $\Pi([\dot{\theta}])$ and (b) $\Pi(\underline{\underline{\dot{\chi}}})$ for a square slab (208 elements)

Figure 10(a) shows the tendency for discontinuities to characterize the rotating 4-block collapse mechanism, including rotational discontinuity along the fixed borders. It is even possible to observe the formation of rigid blocks in the dark blue areas. It can be seen from Fig. 10(b) that near the rotational discontinuity lines located inside the slab there is also bending deformation, which is probably related to the distribution of the triangular elements employed which does not favor the formation of the discontinuity lines in the exact locations. The approximately 1% difference between numerical and analytical solutions of p^+ could be linked to the fact that in the four fixed corners of the slab, there were no rotation discontinuities, which may have contributed to a lower limit value of p^+ for the numerical solution.

Circular slab (radius r) subjected to distributed load simply supported on the boundary. The exact ultimate load solution for a slab with this type of geometry, load and boundary conditions, and strength characterized by Johansen's criterion, is $p^+ = 6M_o \big/ r^2$.

For the numerical solution through the software tool, a circular slab of radius $r = 10m$ was considered. The result for these conditions is $p^+ = 0,06MN\ /\ m^2$. Four distinct finite element meshes were considered, varying the number of elements. The circular slab was approximated by 6,

10, 20 and 30-sided polygons (Fig. 11).

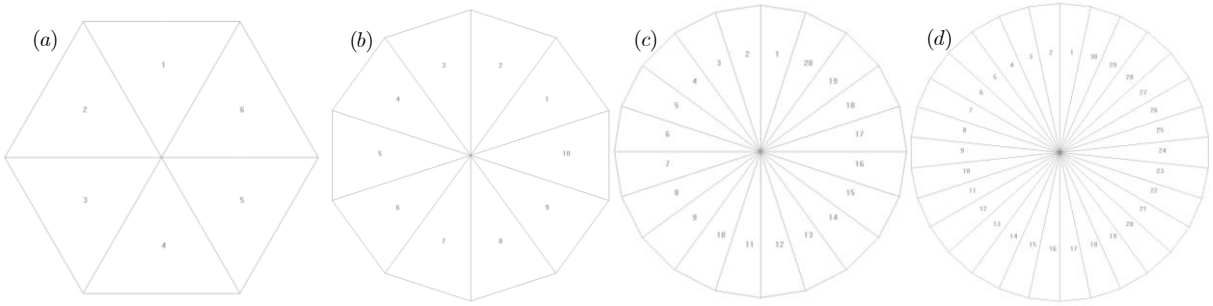

Figure 11. Circular slab meshes: (a) 6, (b) 10, (c) 20 and (d) 30 elements. Source: *GiD®*

The numerical and theoretical results and the relative error for each mesh, can be seen in Table 1. They demonstrated a satisfactory convergence to the theoretical value.

Table 1. Ultimate load for a circular slab and polygonal approximations

Ultimate Load $p^+(MN\ /\ m^2)$				
Theoretical	6-side	10-side	20-side	30-side
0.06	0.080008552	0.066341999	0.061519052	0.060686008
Relative error	33.348 %	10.571%	2.532%	1.143%

Fig. 12 shows the deformed configuration of the circular slab and its "cone collapse mechanism".

Figure 12. Deformed configuration for the circular slab (30 elements).

Circular slab (radius b) with opening (radius a) subjected to linear distributed load on the outer contour, simply supported on the inner bondary. The structure analyzed in this section is represented in Fig. 13. The exact ultimate load solution for the slab with this type of geometry, load and boundary conditions, and strength characterized by Johansen's criterion, is $p^+ = M_o \big/ (b-a)$.

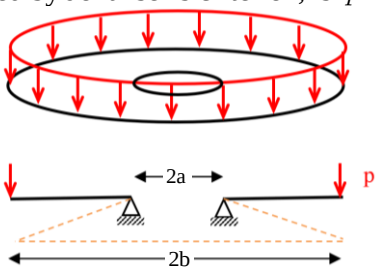

Figure 13. Circular slab with opening simply supported subjected to linear distributed load.

For the analysis, it was considered a circular slab of radiuses $b = 10m$ and $a = 2m$. The theoretical result for this case is $p^+ = 0{,}125MN\ /\ m$. Two distinct finite element meshes were analyzed by varying the number of elements, 20 and 40, referring to approximations of the structure by 12 and 24-sided polygons, respectively, as can be seen in Fig. 14. The numerical and the theoretical results and the relative error for each mesh, can be seen in Table 2. They demonstrated a satisfactory convergence to the theoretical value. In Fig. 15 it is possible to see the deformed configuration of the slab and the collapse mechanism similar to the cone, but inverted.

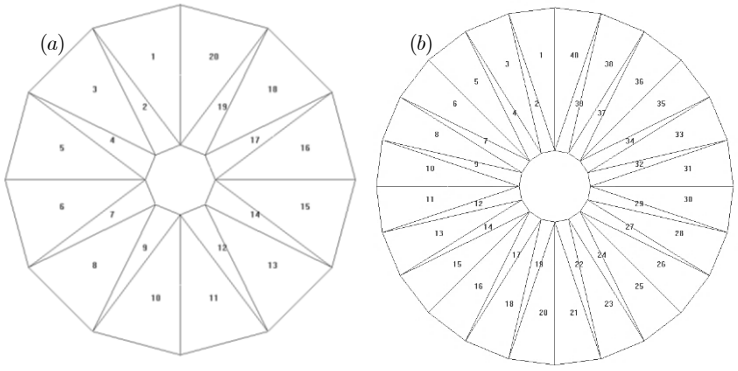

Figure 14. Meshes for a circular slab with opening: (a) 12 and (b) 24 sides polygon. Source: *GiD®*

Table 2. Ultimate load for a circular slab with opening and polygonal approximations

Ultimate Load $p^{+}(MN\ /\ m)$		
Theoretical	14 sides	24 sides
0.125	0.128670789	0.1259955
Relative error	2.937 %	0.797%

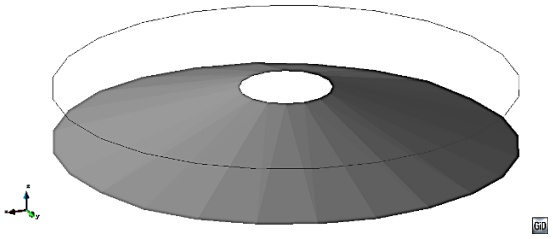

Figure 15. Deformed configuration of a circular slab with opening (24 elements).

5.2 Modelling of Slabs with Known Kinematic Solution

The structures evaluated in this section are known and are frequent slabs in structural projects. They do not have exact analytical solutions, due to the difficulty of finding solutions via static approach. The analytical (kinematic) solutions are presented and compared with the numerical solution obtained by the developed software tool.

Rectangular slab subjected to distributed load, simply supported on the boundary. The structure analyzed in this section and the chosen collapse mechanism are shown in Fig. 16.

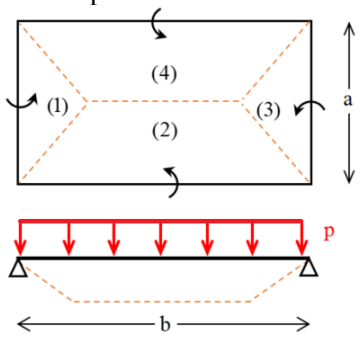

Figure 16. Rectangular slab and the 4-rotation block collapse mechanism.

Through the kinematic approach of the LAT, it is found an upper load limit for the slab with this type of geometry, load distribution, boundary conditions, collapse mechanism, and strength characterized by the Johansen criterion, that is:

$$p^{+} \leq \frac{24M_o}{a^2} \frac{1}{\left(\sqrt{3+\ \lambda\ ^2} - \lambda\right)^2}, \quad with \ \ \lambda = \frac{a}{b}. \tag{14}$$

In this case, two slabs with different λ were analyzed: one slab with 10m x 20m dimensions and another with 10 m x 30 m. The employed meshes can be seen in Fig. 17.

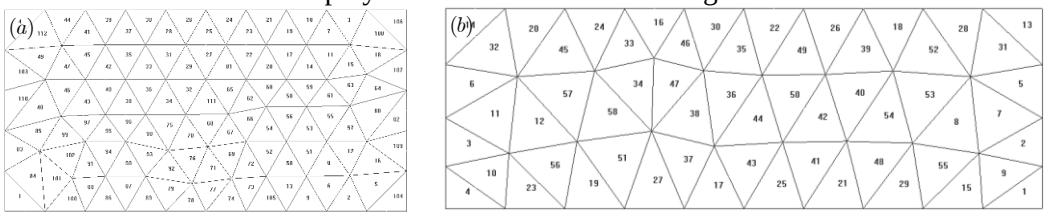

Figure 17. Meshes for a rectangular slab (a) $\lambda = 10/20$ and (b) $\lambda = 10/30$. Source: *GiD®*

The theoretical solutions for both cases as well as the numerical solutions can be seen in Table 3. There is divergence between numerical and theoretical solutions due to the utilized meshes. More refined meshes could allow the formation of the proposed collapse mechanism and even a mechanism that would provide the problem exact solution.

Table 3. Ultimate load for a rectangular slab

Ultimate Load $p^{+}(MN\ /\ m^2)$			
λ	Theoretical	Numerical	Relative Error
$10/20$	0.14141	0.15464707	9.36%
$10/30$	0.11728	0.13508263	15.18%

The isovalues of $\Pi([\dot{\theta}])$ and $\Pi(\dot{\underline{\underline{\chi}}})$ for the case $\lambda = 10/20$ are displayed in Fig. 18(a) and 18(c), respectively, and for the case $\lambda = 10/30$, in Fig. 18(b) and 18(d).

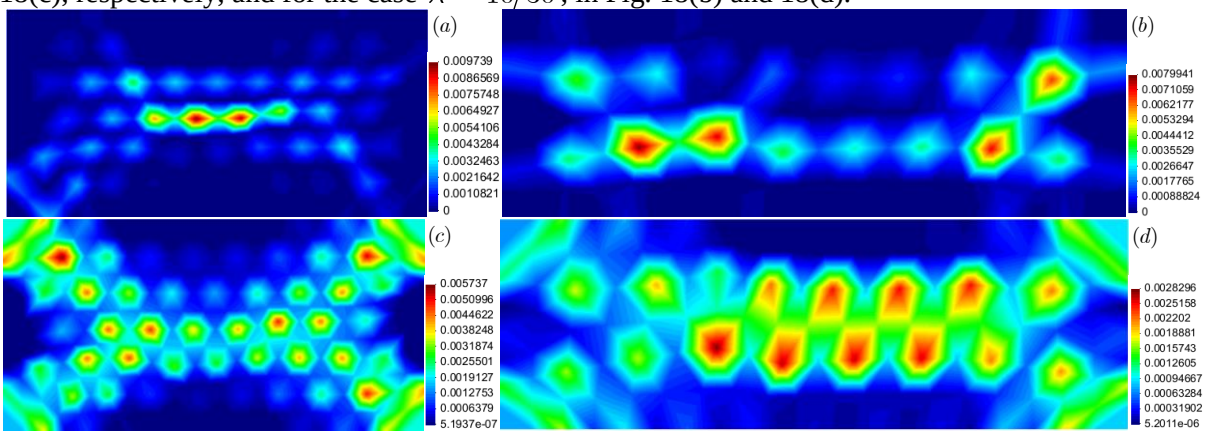

Figure 18. Isovalues of $\Pi([\dot{\theta}])$ and $\Pi(\dot{\underline{\underline{\chi}}})$ for a rectangular slab with $\lambda = 10/20$, (a) and (c) respectively, and with $\lambda = 10/30$, (b) e (d) respectively.

In Figures 18(a) and 18(b) there is a tendency in the two slabs for the development of discontinuity lines similar to the chosen collapse mechanism (Fig. 16). In Figures 18(c) and 18(d), it is observed in both slabs, analogously to the square slab, that the bending deformation seems to compensate for the discontinuities, besides the formation of rigid blocks in the dark blue areas.

Long rectangular slab subjected to a center point load, simply supported on the boundary. For such conditions, it is possible to consider two collapse mechanisms locally occurring in the slab, the first of

a rectangular shape (mechanism 1), and the second with fan-shaped lines (mechanism 2), as illustrated in Figs. 19(a) and 19(b), respectively. Through the kinematic approach of the limit analysis, we find limits for the load of a slab with this type of geometry, load distribution, boundary conditions, collapse mechanisms, and strength characterized by the Johansen criterion, that are $Q^+ \leq 8\sqrt{2}M_o$ *e* $Q^+ \leq M_o(2\pi + 4)$, for mechanisms 1 and 2, respectively.

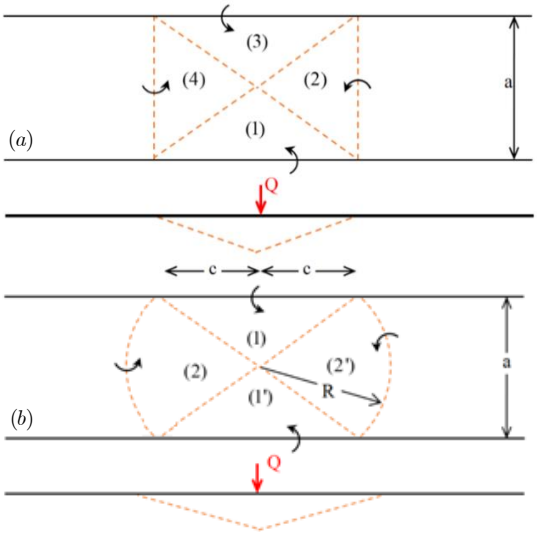

Figure 19. Long rectangular slab and the considered collapse mechanisms 1 and 2.

A 10m x 100m slab was analyzed. The modelled mesh can be seen in Fig. 20.

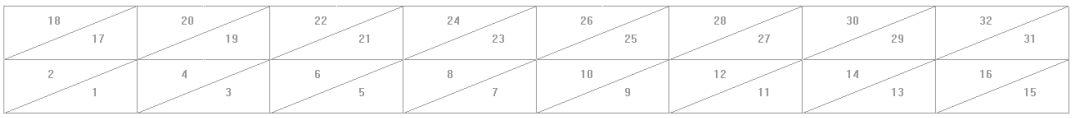

Figure 20. Mesh for a long rectangular slab. Source: *GiD®*

The theoretical solutions for the mechanisms 1 and 2 are 11.81 MN and 10.30 MN respectively, and the numerical solution found by the software was 13.8567 MN. The numerical result represents a relative error of 17.33% relative to mechanism 1 and 34.53% relative to mechanism 2. Figures 21(a) and 21(b) respectively represent the isovalues of $\Pi([\dot{\theta}])$ and $\Pi(\dot{\chi})$.

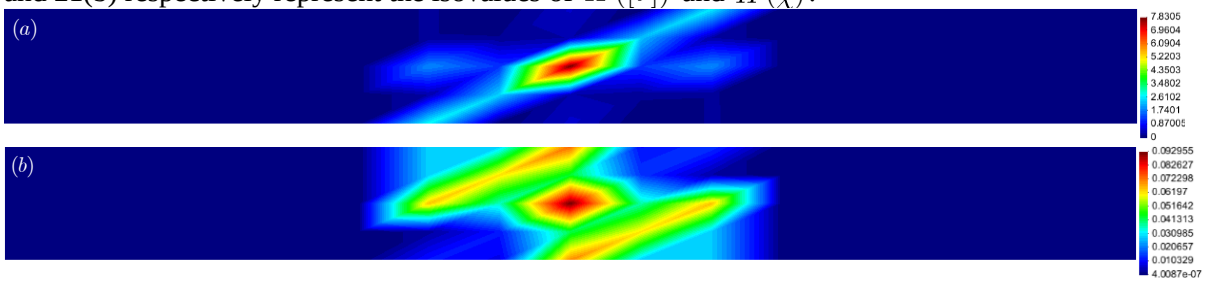

Figure 21. Isovalues of $\Pi([\dot{\theta}])$ and $\Pi(\underline{\underline{\dot{\chi}}})$ for a long rectangular slab.

Figure 21 shows the regions where rotation discontinuities occur (a), which follow the finite element interfaces, and where deformations occur (b). The numerical solution, dependent on the modelled mesh, translates a mixture of collapse mechanism: rotating blocks and cone mechanism. By analyzing a more refined mesh, it would be possible to more clearly observe the discontinuities of rotation and possibly the formation of fan or cone-type mechanisms that combined would establish the exact solution of the problem, as well as reduce the difference found between the ultimate load

numerical and analytic solutions. However, the present work was limited to the free version of *GiD*®.

Triangular slab (equilateral triangle) subjected to a center point load, simply supported on the boundary. For such conditions, it is possible to consider the 3-rigid block collapse mechanism illustrated in Fig. 22. Through the kinematic approach of the limit analysis, we find the load limit for the slab with this type of geometry, load distribution, boundary conditions, collapse mechanism, and strength characterized by the Johansen criterion, that is $Q^{+} \leq 6\sqrt{3}M_{o}$.

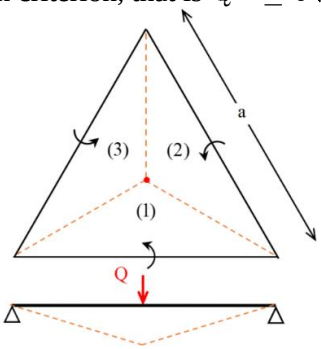

Figure 22. Triangular slab and collapse mechanism of 3 rotating blocks.

An $a = 10m$ side slab was analyzed. The modelled mesh can be seen in Fig. 23.

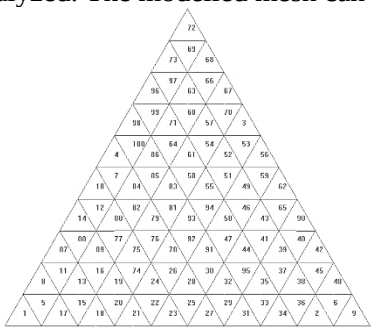

Figure 23. Mesh for a triangular slab. Source: *GiD*®

The theoretical solution for the chosen collapse mechanism is 10.39 MN, and the numerical solution found by the software was 9.837672167 MN, representing a difference of 5.32%. The interpretation of this result is that, there is probably another collapse mechanism for the analyzed structure that results in an upper load limit lower than this known kinematic solution. The mechanism found numerically can be visualized through Figs. 24(a) and 24(b) which represent the isovalues of $\Pi([\dot{\theta}])$ and $\Pi(\dot{\chi})$, respectively.

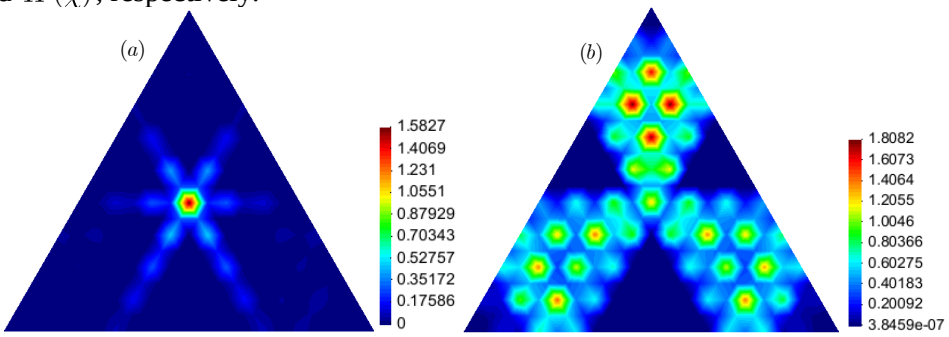

Figure 24. Isovalues of $\Pi([\dot{\theta}])$ and $\Pi(\underline{\underline{\dot{\chi}}})$ for a triangular slab.

Fig. 24 shows that the collapse mechanism combines the rotating rigid blocks and regions with bending deformation, such as a fan-shaped mechanism.

Triangular slab (equilateral triangle) subjected to a center point load, fixed on the contour. For such conditions, it is possible to consider the cone collapse mechanism illustrated in Fig. 25. Through the kinematic approach of the limit analysis, we find the load limit for the slab with this type of geometry, load distribution, boundary conditions, collapse mechanism, and strength characterized by the Johansen criterion, that is $Q^+ \leq 2\pi \;\; M_0^- + M_0^+ \;\;$.

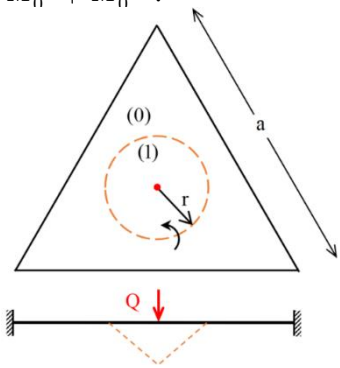

Figure 25. Triangular slab and cone-shaped collapse mechanism.

A slab with the same geometry ($a = 10m$ side) and same mesh previously used for the simply supported slab (Fig. 23) was analyzed. The theoretical solution for this collapse mechanism is 12.57 MN, and the numerical solution found by the software was 13.079058749 MN, representing a difference of 4.05%. The mechanism found can be visualized through Figs. 26(a) and 26(b) which represent the isovalues of $\Pi\,([\dot{\theta}])$ and $\Pi\,(\underline{\underline{\dot{\chi}}})$, respectively.

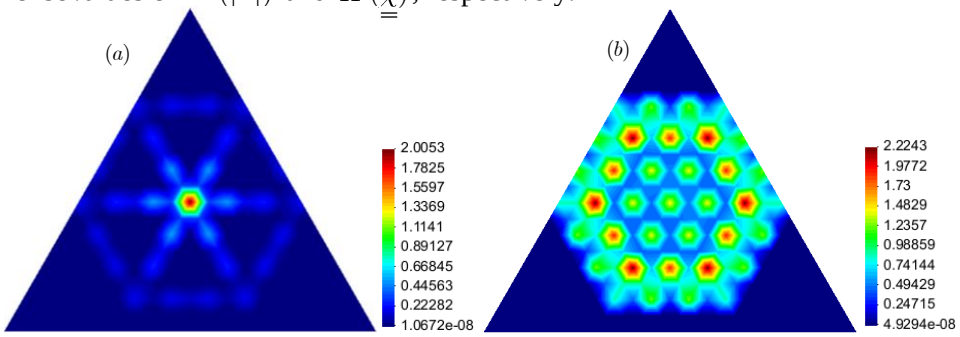

Figure 27. Isovalues of $\Pi\,([\dot{\theta}])$ and $\Pi\,(\underline{\underline{\dot{\chi}}})$ for a triangular slab.

Fig 26 shows that the numerically found collapse mechanism approximates a cone mechanism. Again, the use of a more refined mesh would provide a more accurate collapse mechanism and solution for the ultimate load.

Trapezoidal slab subjected to distributed load, simply supported on the boundary. The structure analyzed in this section and the chosen collapse mechanism are shown in Fig. 27. This mechanism was proposed by Johansen [11] and the upper loading limit for the slab with this type of geometry, load distribution, boundary conditions, collapse mechanism, and strength characterized by the Johansen criterion is (Johansen [11]):

$$p^+ \leq \frac{6 \;\; a+b+c+d \;\; M_o}{r^2 \;\; 3b+3d-a-c}. \tag{14}$$

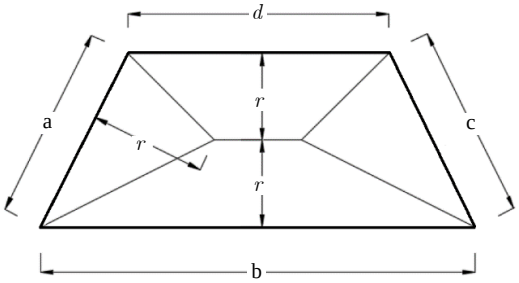

Figure 27. Trapezoidal slab and 4-rotating blocks collapse mechanism.

A slab with $a = c = \sqrt{29}m$, $b = 10m$, $d = 6m$ and $r = 2.5m$ was analyzed. The modelled mesh can be seen in Fig. 28.

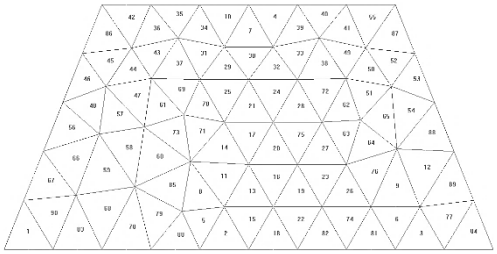

Figure 28. Mesh for a trapezoidal slab. Source: *GiD*®

The theoretical solution for the rupture mechanism is 0.69 MN / m², and the numerical solution found by the software was 0.7181167997 MN / m², representing a difference of 4.075%. The mechanism found can be visualized through Figs. 29(a) and 29(b) which represent the isovalues of $\Pi([\dot{\theta}])$ and $\Pi(\dot{\chi})$, respectively.

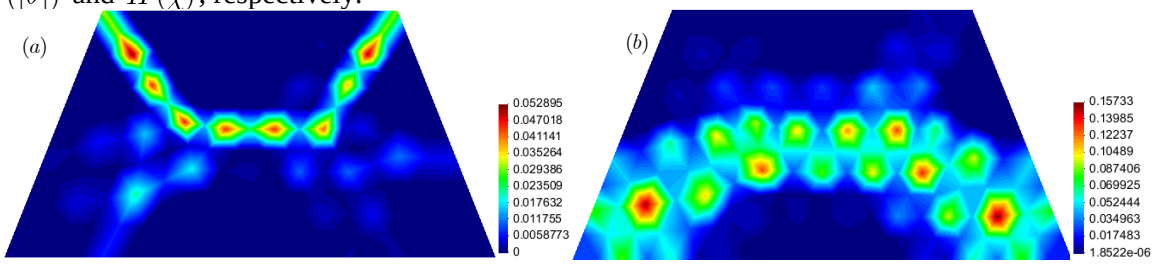

Figure 29. Isovalues of $\Pi([\dot{\theta}])$ and $\Pi(\underline{\underline{\dot{\chi}}})$ for a trapezoidal slab.

It can be seen from Fig 29 that the numerically found collapse mechanism approximates the mechanism proposed by Johansen. It was even found that the value of *r*, theoretically equal to 2.5 m, was numerically obtained as 2.4 m. Come again, the use of a more refined mesh could provide a more accurate collapse mechanism and solution for the ultimate load.

5.3 Modelling of Slabs without Analytical Solution

The choice of the cases addressed in this section, L and T-shaped slabs, was made according to the frequency that such geometries occur in reinforced concrete structure designing.

L-shaped Slab. The analyzed structure in this section, an L-shaped slab of equal panels simply supported along its boundary subjected to distributed load, and the utilized mesh can be seen in Fig. 30.

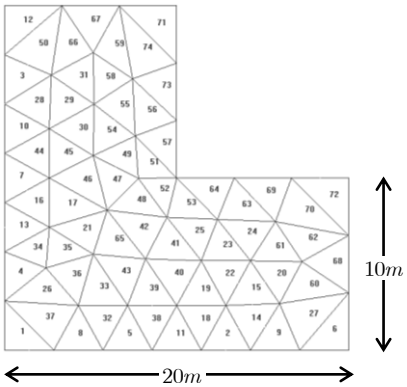

Figure 30. Mesh for an L-shaped slab. Source: *GiD®*

For Oliveira Jr [12], a collapse mechanism solution for this L-shaped slab can be observed in Fig. 31(a). Such solution, L-shaped slab with panels of close dimensions, was given as convergent and the case of equal dimensions panels can be analogically applied. Such study showed no results in terms of ultimate loads. The solution for ultimate load found by the software developed in this work was $p^{+} \leq 0.1521910245\ \mathrm{M}N\ /\ m^{2}$. Figs. 31(b) and 31(c) illustrate the mechanism numerically found. It is observed that the discontinuity lines combined with the bending deformation tend to characterize the mechanism of Oliveira Jr [12]. As in previous examples, the resulting mechanism is the combination of the contributions referring to rotation discontinuities and bending deformation.

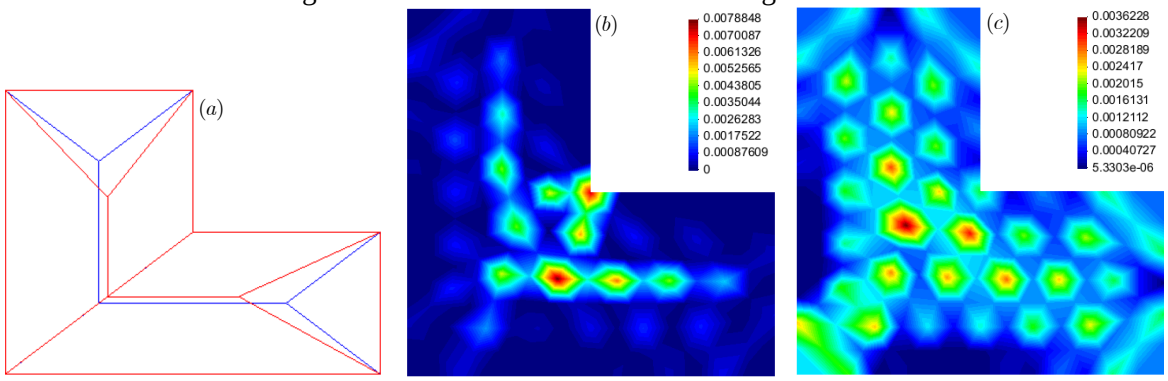

Figure 31. Oliveira Jr Mechanism [12] (a). Isovalues of $\Pi\left([\dot{\theta}]\right)$ (b) and $\Pi\left(\underline{\underline{\dot{\chi}}}\right)$ (c) for L-shaped slab

T-shaped Slab. The analyzed structure in this section, a T-shaped slab of equal panels simply supported along its boundary subjected to distributed load, and the used mesh can be seen in Fig. 32.

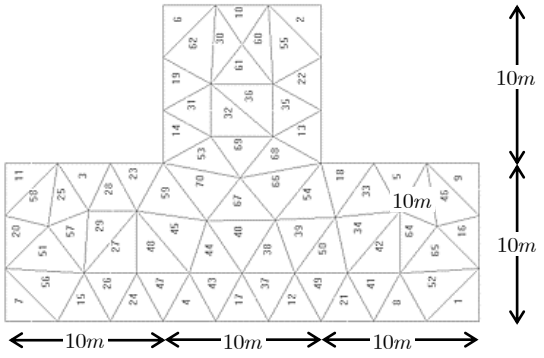

Figure 32. Malha para laje em L. Fonte: *GiD®*

For Oliveira Jr [12], a collapse mechanism solution for this T-shaped slab can be observed in Fig. 33(a). Such solution, for T-shaped slab with panels of close dimensions, was given as convergent and

applicable to the case of equal panels by analogy, as in the case of an L-shaped slab. Such study showed no results in terms of ultimate load. For Pinheiro [13], under simple support conditions, the proposed basic collapse mechanism is that of Fig. 33(b).

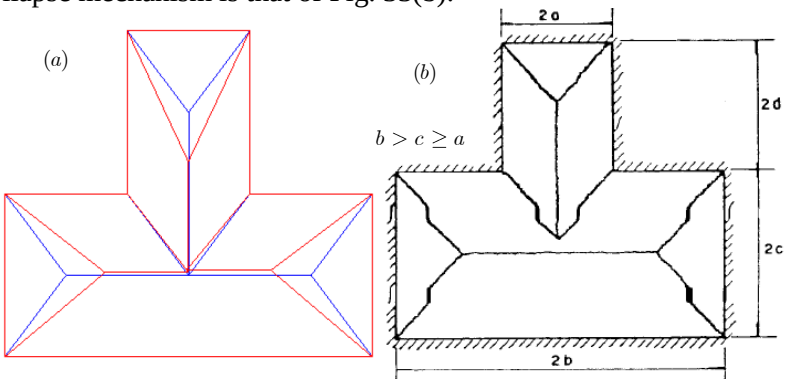

Figure 33. Oliveira Jr [12] (a) and Pinheiro [13] (b) Mechanisms.

The solution for the ultimate load found by the software developed was $p^{+} \leq 0.153116995\ \mathrm{M}N\ /\ m^{2}$. Figs. 34(a) and 34(b) illustrate the mechanism numerically found. Some discontinuity lines seen in the numerical solution are similar to those presented by Oliveira Jr [12] and Pinheiro [13]. The modelled mesh influences the result, which in this case presented a mechanism combining rotation discontinuity with bending deformation. As in previous examples, a more refined mesh could provide a more accurate result.

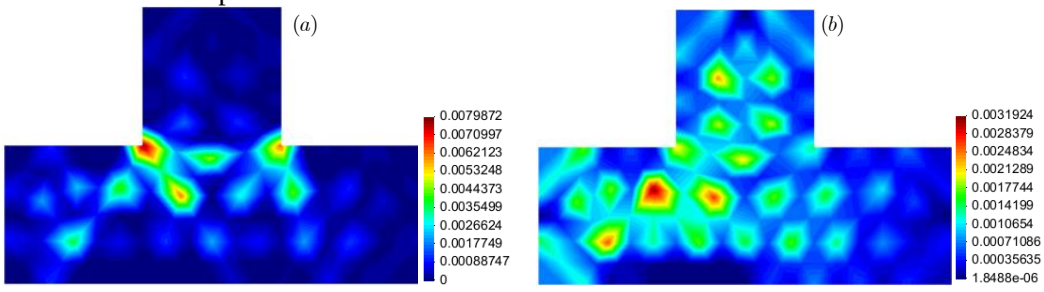

Figure 34. Isovalues of $\Pi([\dot{\theta}])$ (a) and $\Pi(\underline{\underline{\dot{\chi}}})$ for a T-shaped slab (b).

6 Conclusions

This work allowed the development of a software tool that estimates the load capacity of plates and slabs, as well as provides its collapse mechanism. When possible, the problems analyzed were modeled to meet the expected collapse mechanisms, therefore the software tool could converge to the minimum expected solution, or even optimizing such solutions. Due to the adopted method, the pre-processing software generated the meshes and it was not always possible to optimize the distribution of elements so that the analysis of rotation discontinuity lines, or plastic hinges was made precisely.

It can be concluded that the obtained results were satisfactory. The obtained values were practically exact when the mesh modeling allowed the formation of known mechanisms, as in the square and circular slabs cases, and thus, properly approached values and reference mechanisms, in cases with a known solution by the kinematic approach, as in rectangular, triangular and trapezoidal cases. Even in the most complex cases, such as L and T-shaped slabs, the collapse mechanism configurations found by the developed tool were appropriate when compared to mechanisms available in the literature. The most promising result was the simply supported triangular slab result, where the upper load limit value calculated by the software tool was lower than that found through the proposed mechanism, indicating the possibility of estimating a more optimized solution.

Therefore, it is possible to conclude that the tool has a high potential. It can be used as a support

tool for the verification of plates and slabs with geometries distinct of the basic geometries current designed by structural engineers It also can support at the decision-making process, as in the reinforced concrete slabs case, whose geometry implies the need of localized steel reinforcement at regions of concentrated plastification, or plastic hinges. It is noteworthy that this is an embryonic work which demands further studies and improvements. One of them refers to the automation in the use of rougher meshes, which could be itself refined along the calculation process, having as a minimization starting point the results of the previous mesh. In addition, an extensive literature review of experimental works, or even the development of an experimental program for tool calibration and validation would be a valuable contribution and continuation of the proposed work, hence, various plate support and loading conditions can be analyzed and compared with the numerically found results. Finally, the possibility of the future development of a graphical interface for the developed program, simplifying the user-program interaction. Feasibility analysis of such a product is essential for the case of commercial application. The applicability of a tool of this type is easily observable, as solutions for slabs geometries that escape the most basic configurations can be assisted with its support.

References

[1] K. W. Johansen. *Linhas de Ruptura: Teoria e Prática*. (J. Mason). Ao Livro Técnico S.A., 1962.
[2] R. H. Wood and L. L. Jones. *Yield Line Analysis of Slabs.* American Elsevier Publishing Company, 1967.
[3] T. H. M. Langendonck. *Teoria elementar das charneiras plásticas*. ABCP, 1975.
[4] W. F. Chen and D. J. Han. *Plasticity for Structural Engineers*, J. Ross Publishing, 2007.
[5] J. Salençon. *Calcul à la Rupture et Analyse Limite*. Presses de ENPC, 1983.
[6] J. Salençon. *Yield Design*. John Wiley & Sons, Inc., 2013.
[7] O. C. Zienkiewicz, R. L. Taylor and J. Z. Zhu. *The Finite Element Method: Its Basis and Fundamentals.* Elsevier, 2013.
[8] S. S. Rao. *The Finite Element Method in Engineering*. Butterworth-Heinemann, 2010.
[9] J. N. Reddy and D. K. Gartling. *The Finite Element Method in Heat Transfer and Fluid Dynamics*. CRC Press, 2010.
[10] M. Parisotto, Elaboração de um software para determinação via método dos elementos finitos de cargas de ruptura de placas e lajes em flexão Undergraduate Thesis. Federal University of Rio Grande do Sul, 2018.
[11] K. W. Johansen. *Yield-Line formulae for slabs. London*. Cement and Concrete Association, 1972.
[12] I. A. Oliveira Jr. Cálculo de Lajes em Concreto Armado pela Teoria das Linhas de Ruptura: Desenvolvimento de Ferramenta Computacional. Undergraduate Thesis. Federal University of Rio Grande do Sul, 2015.
[13] L. M. Pinheiro, Charneiras Plásticas em Lajes com forma de T – Estudo Experimental. Master Thesis, University of São Paulo, São Carlos, 1980.